doi:10.1093/brain/awx214 BRAIN 2017: 140; 2673–2690 | 2673

BRAIN
A JOURNAL OF NEUROLOGY

# Subarachnoid blood acutely induces spreading depolarizations and early cortical infarction

**Jed A. Hartings,[1,2] Jonathan York,[1] Christopher P. Carroll,[1] Jason M. Hinzman,[1] Eric Mahoney,[1] Bryan Krueger,[1] Maren K. L. Winkler,[3] Sebastian Major,[3,4,5] Viktor Horst,[3] Paul Jahnke,[6] Johannes Woitzik,[7] Vasilis Kola,[3] Yifeng Du,[8] Matthew Hagen,[9] Jianxiong Jiang[8] and Jens P. Dreier[3,4,5]**

See Ghoshal and Claassen (doi:10.1093/brain/awx226) for a scientific commentary on this article.

Early cortical infarcts are common in poor-grade patients after aneurysmal subarachnoid haemorrhage. There are no animal models of these lesions and mechanisms are unknown, although mass cortical spreading depolarizations are hypothesized as a requisite mechanism and clinical marker of infarct development. Here we studied acute sequelae of subarachnoid haemorrhage in the gyrencephalic brain of propofol-anaesthetized juvenile swine using subdural electrode strips (electrocorticography) and intraparenchymal neuromonitoring probes. Subarachnoid infusion of 1–2 ml of fresh blood at 200 μl/min over cortical sulci caused clusters of spreading depolarizations (count range: 12–34) in 7/17 animals in the ipsilateral but not contralateral hemisphere in 6 h of monitoring, without meaningful changes in other variables. Spreading depolarization clusters were associated with formation of sulcal clots ($P < 0.01$), a high likelihood of adjacent cortical infarcts (5/7 versus 2/10, $P < 0.06$), and upregulation of cyclooxygenase-2 in ipsilateral cortex remote from clots/infarcts. In a second cohort, infusion of 1 ml of clotted blood into a sulcus caused spreading depolarizations in 5/6 animals (count range: 4–20 in 6 h) and persistent thick clots with patchy or extensive infarction of circumscribed cortex in all animals. Infarcts were significantly larger after blood clot infusion compared to mass effect controls using fibrin clots of equal volume. Haematoxylin and eosin staining of infarcts showed well demarcated zones of oedema and hypoxic-ischaemic neuronal injury, consistent with acute infarction. The association of spreading depolarizations with early brain injury was then investigated in 23 patients [14 female; age (median, quartiles): 57 years (47, 63)] after repair of ruptured anterior communicating artery aneurysms by clip ligation ($n = 14$) or coiling ($n = 9$). Frontal electrocorticography [duration: 54 h (34, 66)] from subdural electrode strips was analysed over Days 0–3 after initial haemorrhage and magnetic resonance imaging studies were performed at ~24–48 h after aneurysm treatment. Patients with frontal infarcts only and those with frontal infarcts and/or intracerebral haemorrhage were both significantly more likely to have spreading depolarizations (6/7 and 10/12, respectively) than those without frontal brain lesions (1/11, $P$'s $< 0.05$). These results suggest that subarachnoid clots in sulci/fissures are sufficient to induce spreading depolarizations and acute infarction in adjacent cortex. We hypothesize that the cellular toxicity and vasoconstrictive effects of depolarizations act in synergy with direct ischaemic effects of haemorrhage as mechanisms of infarct development. Results further validate spreading depolarizations as a clinical marker of early brain injury and establish a clinically relevant model to investigate causal pathologic sequences and potential therapeutic interventions.

1 Department of Neurosurgery, University of Cincinnati College of Medicine, Cincinnati, OH, USA
2 UC Gardner Neuroscience Institute and Mayfield Clinic, Cincinnati, OH, USA
3 Center for Stroke Research Berlin, Charité University Medicine Berlin, Germany
4 Department of Neurology, Charité University Medicine Berlin, Germany
5 Department of Experimental Neurology, Charité University Medicine Berlin, Germany
6 Department of Radiology Charité University Medicine Berlin, Germany
7 Department of Neurosurgery, Charité University Medicine Berlin, Germany
8 Division of Pharmaceutical Sciences, University of Cincinnati College of Pharmacy, Cincinnati, OH, USA
9 Department of Pathology and Laboratory Medicine, University of Cincinnati College of Medicine, Cincinnati, OH, USA

Received January 4, 2017. Revised June 16, 2017. Accepted July 10, 2017. Advance Access publication September 6, 2017

Correspondence to: Jed A. Hartings, PhD
Department of Neurosurgery
University of Cincinnati
231 Albert Sabin Way
Cincinnati, OH 45267, USA
E-mail: jed.hartings@uc.edu

**Keywords:** aneurysmal subarachnoid haemorrhage; brain infarction; cortical spreading depression; electroencephalography; intensive care

**Abbreviations:** ACI = acute cerebral ischaemia; COX-2 = cyclooxygenase-2; ECoG = electrocorticography; ICH = intracerebral haemorrhage; $P_{bt}O_2$ = brain partial pressure of oxygen; PTDDD = peak total depression duration per day; SAH = subarachnoid haemorrhage; TDDD = total depression duration per day

# Introduction

Research in aneurysmal subarachnoid haemorrhage (SAH) has predominantly focused on delayed cerebral ischaemia and vasospasm. These complications arise between Days 5 to 14, are accompanied by new onset neurological deficits and cerebral infarction, and are therefore attractive targets for early detection and timely intervention to improve outcomes. However, delayed cerebral ischaemia accounts for only 13% mortality, in contrast to 86% of deaths associated with the initial injury before this period (Broderick *et al.*, 1994), termed acute cerebral ischaemia (ACI) (Sarrafzadeh *et al.*, 2002). ACI describes the initial neurological deficits after SAH, which are important determinants not only of initial survival but also morbidity and long-term outcome (Lagares *et al.*, 2001; Claassen *et al.*, 2002; Sarrafzadeh *et al.*, 2002; Sakowitz *et al.*, 2013).

An important aspect of ACI is the presence of acute ischaemic brain lesions frequently observed in patients who present with poor grade (Hadeishi *et al.*, 2002; Wartenberg *et al.*, 2011; De Marchis *et al.*, 2015). For instance, up to 85% of patients with Hunt-Hess classification of 4–5 had cortical lesions on diffusion-weighted imaging (DWI) within 96 h of SAH onset (Wartenberg *et al.*, 2011), and the presence of early lesions (<48 h) is associated with worse neurologic status on admission and also worse long-term outcomes (De Marchis *et al.*, 2015). These lesions typically are bilateral, patchy, and multifocal, occur in laminar cortical patterns, are often present in the anterior cerebral artery territory, and are not related to intracerebral haemorrhage (ICH). Autopsy studies reveal similar findings (Neil-Dwyer *et al.*, 1994). Early ischaemic lesions are under-appreciated, as they often cannot be observed on CT scans (Dreier *et al.*, 2002; Schmidt *et al.*, 2007; Wartenberg *et al.*, 2011).

ACI and cortical ischaemic lesions have been hypothesized to result from increased intracranial pressure and intracranial circulatory arrest at the time of aneurysm rupture, ultra-early vasospasm, or local vessel thrombosis (Sehba and Bederson, 2006; Lee *et al.*, 2010; Wartenberg *et al.*, 2011; Terpolilli *et al.*, 2015). Another concept is based on the observation that patchy, laminar infarcts show 'a preference for the circumvolutions in the area of the subarachnoid haemorrhage' (Stoltenburg-Didinger and Schwarz, 1987) and occur in band-like patterns around sulci and fissures (Dreier *et al.*, 2002). Indeed, several studies have observed cortical infarcts in regions of subarachnoid blood accumulation (Weidauer *et al.*, 2008; Wagner *et al.*, 2013). Accordingly, a proposed mechanism is that erythrocyte breakdown products provoke waves of spreading depolarization in the cortex and, by disrupting normal neurovascular coupling, also cause a pathologic vasoconstrictive response to depolarization known as spreading ischaemia (Dreier *et al.*, 1998; Dreier, 2011; Ayata and Lauritzen, 2015). It was shown that application of haemolysis products to rat cerebral cortex results in laminar infarcts through the spreading depolarization and spreading ischaemia mechanisms (Dreier *et al.*, 2000). This concept was translated to patients by documenting a delayed period (Days 5–9) of repetitive spreading depolarizations that predicted the onset of delayed cerebral ischaemia, including neurologic deficits and new cortical lesions (Dreier *et al.*, 2006, 2009; Drenckhahn *et al.*, 2012). However, an earlier peak of spreading depolarizations is also observed on Days 0–2 in SAH patients (Dreier *et al.*, 2012). Therefore, we hypothesized that spreading depolarizations may also be involved in the development of early cortical infarction in the period of ACI.

Here we used a swine model to determine whether focal accumulation of subarachnoid blood is a sufficient insult to acutely induce repetitive spreading depolarizations, as first suggested by Hubschmann and Kornhauser (1980, 1982). In contrast to commonly used rodent models, the gyrencephalic swine brain more closely models the subarachnoid spaces of sulci and fissures in humans, where blood accumulates, clots, and persists in substantial volumes. We find that sulcal subarachnoid clots not only induce repetitive spreading depolarizations, but also cause infarction of adjacent cortex in patterns similar to those observed clinically. In a focused clinical study, we further found a robust association between the occurrence of spreading depolarizations and cortical lesions in the acute phase after

aneurysmal SAH. Together, these results suggest spreading depolarization as a marker and mechanism of developing ACI.

# Materials and methods

## Swine study

Experiments were initiated to determine whether subarachnoid blood is sufficient to induce spreading depolarization in the gyrencephalic brain. Since novel methods were used and preliminary data were not available, sample sizes were not predetermined. Animals were excluded if surgical manipulations caused traumatic parenchymal injury ($n = 5$). Outliers were not excluded. Analysis of the relationship of infarcts to spreading depolarization was retrospective and unblinded, since infarction was not an anticipated, prospective endpoint. Results are reported in accordance with ARRIVE guidelines.

### Animal care, preparation, and surgical procedures

Fourty-one female juvenile domestic swines weighing 32–40 kg were housed singularly and food and water were provided *ad libitum* for at least 2 days prior to experimental procedures. Procedures were conducted under a protocol approved by the University of Cincinnati Institutional Animal Care and Use Committee and conformed to the NIH Guide for the Care and Use of Laboratory Animals. After fasting for 12 h, anaesthesia was induced with intramuscular xylazine (1 mg/kg), telazol (4–7 mg/kg), and atropine (0.04 mg/kg). Animals were intubated and ventilated with medical air ($FiO_2$ 30%) and anaesthesia maintained with isoflurane (2–5%). A femoral artery was cannulated (18 g) for blood withdrawal, sampling, and pressure monitoring. Electrocardiogram was recorded, capillary oxygen saturation ($SpO_2$) was monitored at the nares, and core temperature maintained at 36–37°C. Ear veins were then cannulated (18 g), isoflurane discontinued, and anaesthesia maintained throughout subsequent cranial surgery and neuromonitoring with intravenous propofol (6 ml/kg bolus followed by 15–25 mg/kg/h infusion). Ringer's lactate solution was given continuously at 75 ml/h, and depth of anaesthesia was monitored by reflexes, muscle relaxation, blood pressure, and heart rate. When required, anaesthesia was increased with a 2–3 ml propofol bolus and 5 mg/kg/h increase of infusion rate. Animals were then placed in the prone position for the remainder of the study. The scalp was retracted and large and small craniotomies were made for blood/clot infusion and placement of subdural electrode strips and intracranial monitors, respectively (Fig. 1A).

### Experimental procedures and monitoring

Electrode strips (platinum, six-contact, 10-mm spacing; Wyler, Ad-Tech Medical) were placed through small anterior craniotomies and positioned over the superior frontal gyrus medial to the cruciate sulcus (Fig. 1B), following previous anatomic nomenclature (Yun *et al.*, 2011; Schmidt, 2015). After baseline recordings, the ipsilateral strip was moved to allow unrestricted access to the arachnoid mater covering the superior frontal and motor gyri and cruciate and diagonal sulci through the large craniotomy site, and SAH or control infusion was induced by procedures described below. Immediately after SAH, the strip was repositioned and a quad-lumen bolt (Hemedex, Inc) was secured in the burr hole adjacent to the craniotomy. Brain temperature, intracranial pressure, and brain partial pressure of oxygen ($P_{bt}O_2$) were monitored with a single probe (Neurovent-PTO) and regional cerebral blood flow by a thermal diffusion probe (QFlow 500, Hemedex, Inc) passed through the bolt. Craniotomies were sealed with bone wax.

Animals were then monitored continuously for 6 h until euthanasia. Arterial blood gases were sampled at the start and end of monitoring (i-STAT 1) and arterial blood biochemistry was analysed by Antech Diagnostics. EKG, $SpO_2$, blood pressure, intracranial pressure, $P_{bt}O_2$, and brain temperature were monitored on a Phillips Intellivue MP50 and recorded with waveform resolution on a CNS-200 (Moberg Research, Inc). Electrocorticography (ECoG) was recorded directly to the CNS-200 through a direct current (DC)-coupled amplifier. Monopolar recordings were referenced to an epidural platinum electrode over the contralateral hemisphere and ground was provided by a Ag/AgCl electrode on the neck. At the end of the monitoring period, animals were euthanized by an intravenous bolus of pentobarbital (150–200 mg/kg).

### Subarachnoid haemorrhage and controls

The effects of subarachnoid blood infusion were studied using either fresh (Cohort 1) or clotted (Cohort 2) autologous arterial blood. For Cohort 1, blood was drawn from the femoral catheter into a heparinized syringe and infused with a syringe pump (Fusion 400, Chemyx) through 3 ft of tubing. Under a surgical microscope, the needle (27 or 30 gauge) was manually inserted ~2 mm through the arachnoid between the crests of the superior frontal and motor gyri (Fig. 1B) and 1 ml of blood was slowly infused over 5 min (12 ml/h). For some animals, the procedure was repeated to infuse an additional 1 ml of blood into the diagonal sulcus, laterally adjacent across the motor gyrus. For Cohort 2, fresh arterial blood was placed in dishes and allowed to clot for 30–60 min in an incubator at 37°C. Clotted components were then drawn into a 3 ml plastic syringe, taking care to exclude unclotted blood and serum. A 4 mm incision was made through the arachnoid over the cruciate sulcus, between superior frontal and motor gyri, using a no.11 blade scalpel, and a blunt probe was used to explore the sulcus and ensure space for clot injection. The blunt syringe tip (4 mm o.d.) was then inserted ~7 mm into the sulcus and 1 ml of clotted blood was ejected over 1 min. Estimation of free haemoglobin in blood infusions is described in the Supplementary material. The same surgical procedures were used in control experiments for Cohort 2, but with sulcal injection of normal saline (surgical control) or fibrin sealant (Tisseel®, Baxter Pharmaceuticals; mass effect control). The latter was infused using the supplied syringe filled with fibrinogen and thrombin, which mix upon injection to form a fibrin clot.

### Post-mortem studies

Animals were decapitated following euthanasia and brains were harvested, placed in an ice-cold saline bath for 10 min, and sliced coronally in 5-mm sections (Pig Brain Slicer Matrix, Zivic Instruments). Slices were placed in a 1% TTC (2,3,5-triphenyltetrazolium hydrochloride) (Sigma Aldrich) saline

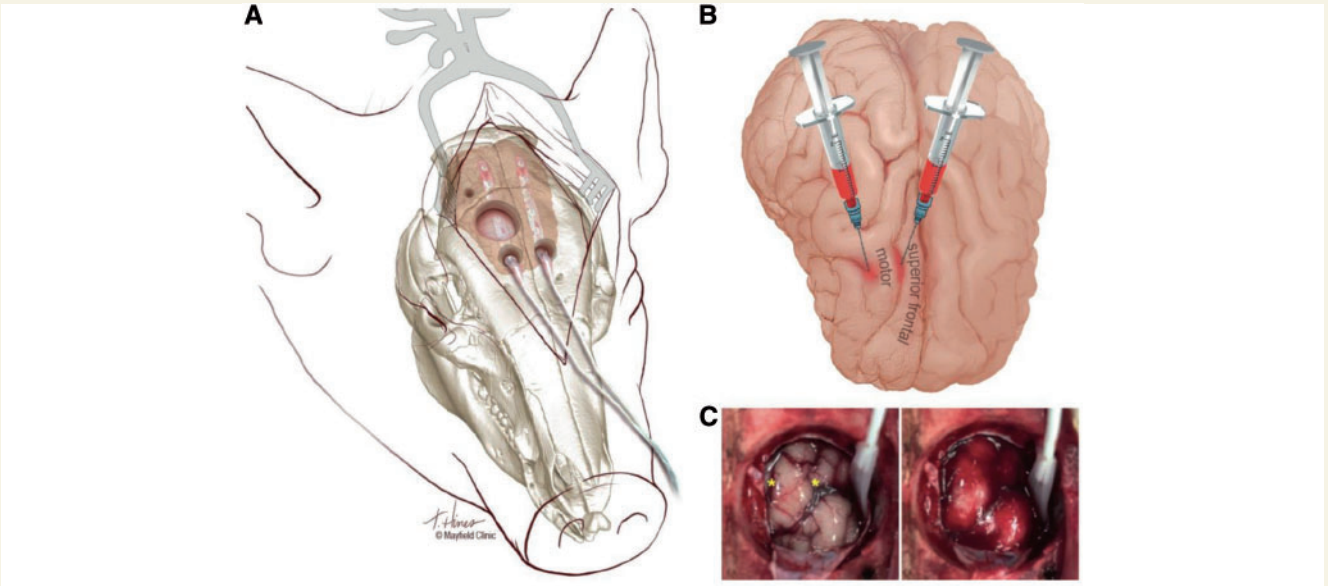


**Figure 1 Swine model of subarachnoid haemorrhage.** (**A**) Illustration of the surgical preparation and subdural electrode strip monitoring. For subarachnoid blood infusion, a large (22 mm) craniotomy was made using a power drill and then a curette and Kerrison punches, abutting the sagittal suture medially and reaching 5 mm anterior to the coronal suture posteriorly. The dura was opened with a no.11 blade scalpel and reflected, taking care to avoid bridging veins. Smaller burr holes 5-mm anterior to the large craniotomy, made using a manual twist drill (8 mm bit) and widened mediolaterally with a Kerrison punch, were used to introduce 6-contact electrode strips. A no.3 Penfield was used to protect the cortex and guide placement in the subdural space. Intraparenchymal blood flow, pressure, temperature, and oxygen sensors were placed through a small burr hole immediately posterior and lateral to the large craniotomy. (**B**) Illustration depicts the locations of blood injection into two sulci medial and lateral to the motor gyrus. Fresh autologous blood was injected at one or both locations in Cohort 1 animals, while clotted blood was injected into the medial (cruciate) sulcus in Cohort 2 animals. Dorsal view: anterior is down. (**C**) Photographs of the brain surface through the large craniotomy before (*left*) and after (*right*) infusion of 1 ml of fresh blood at each location (yellow stars). The electrode strip was subsequently positioned for continuous monitoring. Anterior is up, medial left. Illustrations by Tonya Hines, printed with permission from Mayfield Clinic.

buffer solution at 37°C for 60 min and digitally imaged. Areas of infarction were defined as those lacking red TTC stain, and total infarct volumes were computed by integrating infarct areas of sequential brain sections. Clots were measured as maximal thickness perpendicular to the sulcal plane among all slices. For histological processing, sections were then fixed in 4% paraformaldehyde for 24 h and, following three 30-min washes in phosphate-buffered saline (PBS) at 4°C, dehydrated by serial immersion in 10% (12 h), 20% (24 h) and 30% (24 h) sucrose at 4°C. Tissue was cryoprotected in a 1:1 ratio of 30% sucrose and Neg-50™ (Fisher Scientific) for 4 h at 4°C and then snap-frozen and stored at −80°C. Thin (8–20 µm) sections were cut on a cryostat, mounted on SuperFrost® Plus slides, and stained with haematoxylin and eosin (Sigma Aldrich). Procedures for immunoblotting, RT-PCR, and immunohistochemistry are reported in the Supplementary material.

## Clinical study

For the clinical study, we selected patients from a prospectively collected database using pre-specified criteria and endpoints, as described below. The protocol was approved by the ethics committee of the Charité University Medicine Berlin. Either informed consent or surrogate informed consent was obtained for all patients, and research was conducted in accordance with the Declaration of Helsinki. Results are reported in accordance with STROBE guidelines.

### Patient selection and characterization

Patients with aneurysmal SAH consecutively enrolled in the COSBID (Co-Operative Studies on Brain Injury Depolarizations) study at two centres (Campus Virchow Klinikum and Campus Benjamin Franklin, Berlin, Germany) were screened for study inclusion. Prospective inclusion criteria for COSBID have been described previously (Drenckhahn *et al.*, 2013; Winkler *et al.*, 2017). For this study, patients were further screened retrospectively for ruptured aneurysms of the anterior communicating artery and the availability of an early MRI scan performed between ~24 and ~48 h after aneurysm treatment. Twenty-three patients enrolled between September 2009 and February 2013 met the criteria—12 at one site and 11 at the other. Eight cases were previously reported (Winkler *et al.*, 2017).

Aneurysms were assessed using four-vessel digital subtraction angiography, or more restricted studies when indicated. Haemorrhage was graded according to the original Fisher scale (Fisher *et al.*, 1980) and the modified Hijdra Sum Scale for the global and local SAH burden (Bretz *et al.*, 2016). After aneurysm treatment, patients were transferred to intensive care where continuous neuromonitoring commenced. Glasgow Coma Scale, blood gases, glucose and electrolytes were documented at least every 6 h. Thorough neurological examinations

and transcranial Doppler sonography were performed daily and oral nimodipine was given prophylactically.

### Neuroimaging

MRI was performed on 1.5 T scanners. Sequences used for analysis were $T_1$ multiplanar reconstruction, $T_1$ spin-echo, $T_2$*, $T_2$ turbo inversion recovery magnitude (TIRM), and DWI including apparent diffusion coefficient mapping. Slice thicknesses were 6 mm except for $T_1$ multiplanar reconstruction (1 mm). The early post-interventional MRI scan was analysed by V.H. and P.J. in a blinded fashion. Since the aim was to study brain injury in the vicinity of the bleeding source (anterior communicating artery), only the frontal lobe territory of the anterior cerebral artery was assessed; other regions were not taken into consideration. For analysis, the region of interest was first classified into normal, ischaemic or haemorrhagic for each patient using all sequences including DWI and apparent diffusion coefficient mapping. The volume of ischaemic infarction was then quantified on $T_2$ TIRM images and the ICH volume was quantified on $T_2$* images using Clusterize. Clusterize is a semi-automated, iterative algorithm that has been validated for lesion demarcation in stroke (de Haan *et al.*, 2015).

### Electrocorticography and neuromonitoring

For continuous ECoG recordings, a six-contact platinum electrode strip (see above) was placed on cerebral cortex accessible either through craniotomy during aneurysm surgery or via extended burr hole (Dreier *et al.*, 2009). The near-DC/AC-ECoG (0.01–45 Hz) was recorded in five bipolar channels with a GT205 amplifier (ADInstruments). A subdermal platinum needle electrode was used as reference for additional monopolar recordings, and in some cases full-band ECoG (0–45 Hz) was also measured (BrainAmp MR plus, Brain Products). Data were sampled at 200 Hz and recorded and analysed with a Powerlab 16/SP and Chart-7 software (ADInstruments). $P_{bt}O_2$ was recorded in eight patients using a Clark-type intraparenchymal sensor (Licox CC1P1, Integra) (Winkler *et al.*, 2017). Intracranial pressure was monitored via ventricular drainage catheter or intracranial pressure transducer (Codman or Camino systems). Arterial pressure was recorded from the radial artery.

### Electrocorticography analysis

ECoG analyses were performed by M.K.L.W. with blinding to the clinical courses and neuroimaging findings, and were discussed with J.P.D. The first 24-h period was denoted as 'Day 0'. Only recordings from the early time window of ACI (Days 0–3) were analysed. Spreading depolarizations were identified by the consecutive occurrence of DC shift (slow potential changes) in the DC/near-DC range ($<0.05$ Hz) of neighbouring ECoG channels. In electrically active tissue, spreading depolarization typically causes spreading depression of spontaneous activity in the AC-ECoG range (0.5–45 Hz) (Dreier *et al.*, 2006). Spreading depolarizations were counted and depression durations were scored to measure the total number of spreading depolarizations per recording day (spreading depolarizations/day) and the total depression duration per recording day (TDDD), following established COSBID procedures (Dreier *et al.*, 2017). The peak spreading depolarizations/day and peak TDDD (PTDDD) were defined for each patient as the maximal values among all recording days. Ictal epileptiform events (IEEs) and baseline values of $P_{bt}O_2$, cerebral perfusion pressure, mean arterial pressure, intracranial pressure and heart rate were also scored as previously described (Winkler *et al.*, 2017).

## Statistics

Data in the text are given as median (first, third quartile). All tests are stated in the 'Results' section and were two-sided, and $P < 0.05$ was accepted as statistically significant.

# Results

Experiments were conducted in two cohorts of mechanically ventilated juvenile swine under propofol anaesthesia. Supplementary Table 1 shows the arterial blood gases, biochemistry, and blood counts for both cohorts, which were similar to each other and in normal ranges for juvenile swine.

## Subarachnoid infusion of fresh arterial blood induces spreading depolarizations and infarction

In the first cohort ($n = 17$), fresh autologous blood (1 ml) was infused (200 µl/min) at two locations in nine animals, at a single location in six, and 2 ml was infused at a single location in two others. Blood was infused over sulci between gyral crests and was observed to gradually fill the subarachnoid space during the procedure (Fig. 1B and C). Results were variable in the formation of clots, cortical infarcts and the occurrence of spreading depolarizations, but did not vary by injection protocol; therefore, results for different protocols were pooled. Free plasma haemoglobin of the infused blood was estimated at 0.48 (± 0.42) g/dl ($n = 5$).

Infusion of fresh blood resulted in continuous, repetitive spreading depolarizations (range: 12–37) throughout the 6-h post-SAH monitoring period in 7/17 (41%) animals (Fig. 2D). ECoG monitoring began after 5–10 min and the first spreading depolarization was observed after a median duration of 22 min (quartiles: 12, 30). Spreading depolarizations typically spread widely throughout the ipsilateral hemisphere (Fig. 3). All spreading depolarizations in these animals occurred at inter-depolarization intervals $<30$ min and thus occurred in temporal clusters (Dreier *et al.*, 2006; Hertle *et al.*, 2012). Using 30-s binning, modal intervals for individual animals ranged from 8.5–9.0 to 15.0–15.5 min, and the modal interval for the group was 11.0–11.5 min. In the remaining animals, spreading depolarizations were not observed ($n = 4$) or occurred only as isolated events in sparse numbers (count range: 1–6; $n = 6$). The hemisphere contralateral to subarachnoid blood injection was also monitored in 10 animals and no spreading depolarizations were observed (Fig. 3).

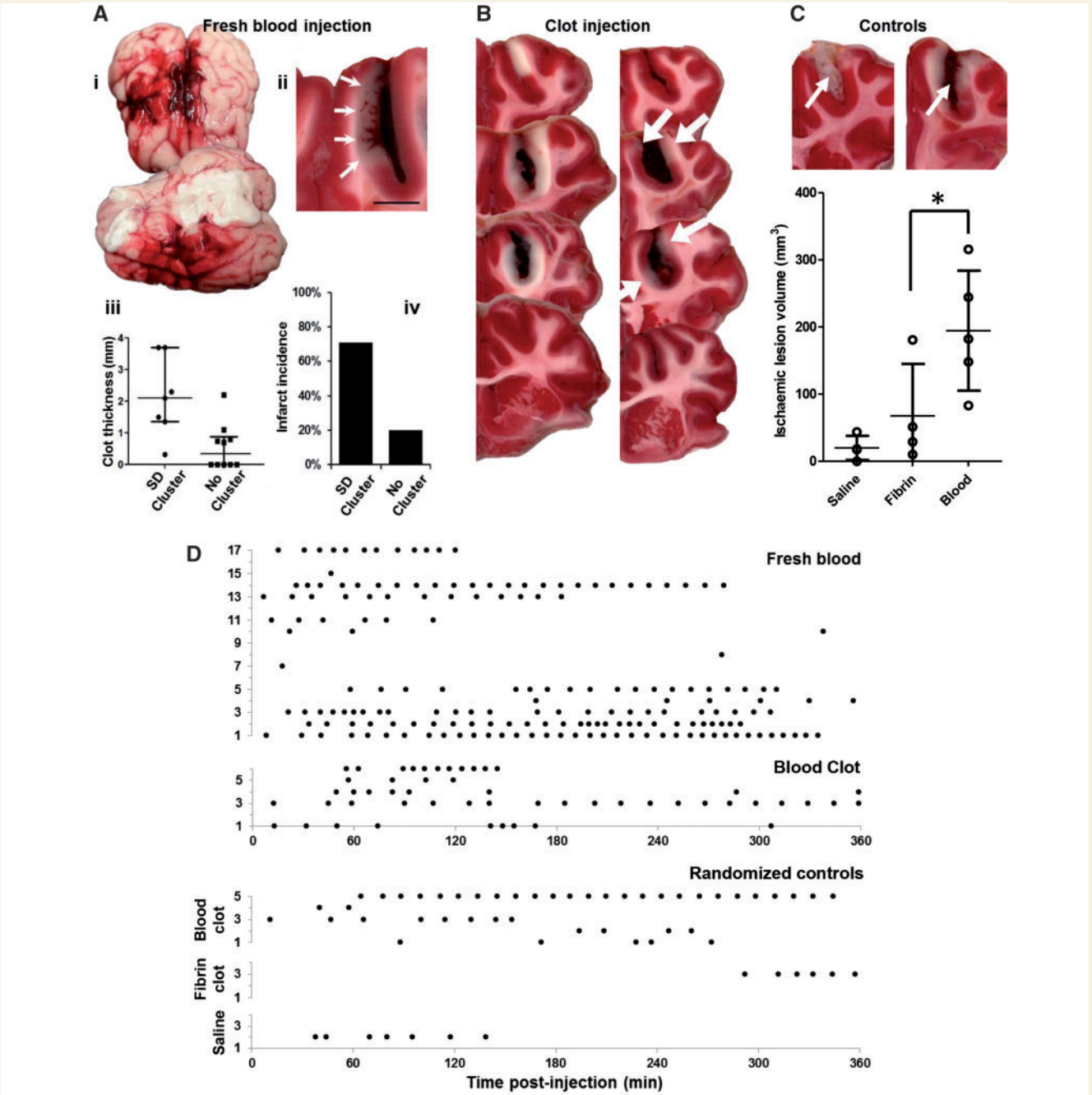


**Figure 2 Spreading depolarizations and pathology following subarachnoid haemorrhage in the swine.** (**A**) Cohort 1 experiments using fresh blood. (**i**) Gross pathology after 6 h showing the persistence and spread of subarachnoid blood through the injected (right) hemisphere, including presence along the Sylvian fissure and ventrolateral surface, as well as surface midline structures of both hemispheres. (**ii**) TTC-stained coronal section shows subarachnoid clot formation in the cruciate sulcus with infarction (arrows) of the medially adjacent cortex. Infarcted cortex lacks red TTC stain. Scale bar = 5 mm. (**iii**) Scatter plots of sulcal clot thickness and (**iv**) infarct incidence for animals with spreading depolarization (SD) clusters ($n = 7$) and animals with sparse or no spreading depolarizations ($n = 10$). Bars in **iii** show median and quartiles. (**B**) Cohort 2 experiments using clotted blood. Sequential 5-mm TTC-stained coronal sections show sulcal subarachnoid clots and adjacent cortical infarction in two representative animals. In the *right* image, the cortex is infarcted around the full extent of the clot, including the sulcal depth, and even extends anteriorly (*top section*) beyond the clot. In the *left* image infarcts (white arrows) are scattered, less extensive, and discontinuous, though present only adjacent to the clot. (**C**) Ischaemic lesion volumes following randomization to sulcal injection of saline, fibrin sealant, or clotted blood. Bars show means and standard deviations (*$P < 0.05$; see text). Upper images of TTC staining from fibrin (*left*) and blood clot (*right*) animals demonstrate the similarity of sulcal clot volumes (arrows) between the groups. (**D**) Raster plots show the timing of individual spreading depolarizations for each animal in Cohort 1 (fresh blood), Cohort 2 (blood clot), and randomized control groups.

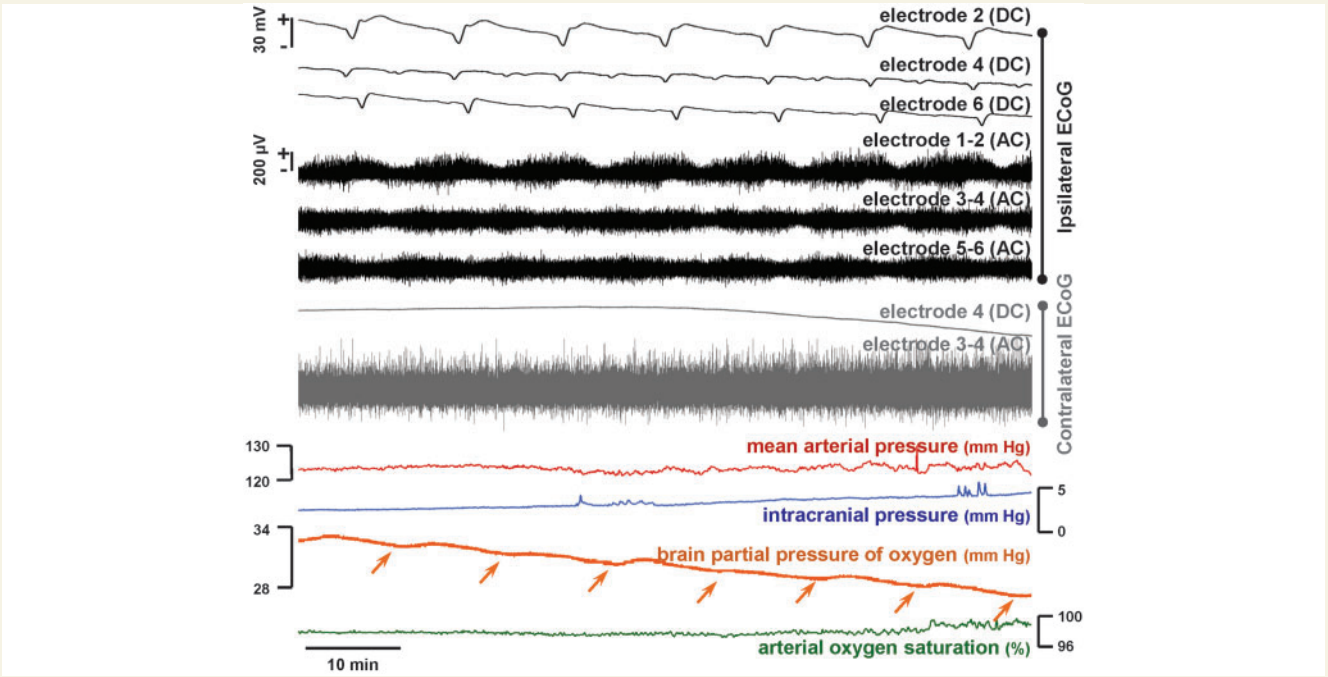


**Figure 3 Representative cluster of spreading depolarizations in the ipsilateral hemisphere following subarachnoid infusion of fresh blood in the swine brain.** Black traces show ECoG recordings from the subdural strip in the hemisphere of blood injection, while grey traces show representative contralateral recordings. Monopolar direct current (DC) recordings show negative DC shifts (slow potential changes), as the signature of spreading depolarization, propagating across the entire ipsilateral hemisphere, while bipolar recordings of high frequency (alternating current, band-pass 0.5–50 Hz) activity show the associated depression periods. Seven spreading depolarizations are observed in this 77-min period (interspreading depolarization interval ~11 min); a total of 34 were observed in 6 h of monitoring. No spreading depolarizations were observed contralaterally. Other neuromonitoring variables remained within normal ranges throughout the experiment, although brain oxygenation levels decreased slightly in a stepwise manner (arrows) with the passage of each spreading depolarization, reaching 20 mmHg at the time of sacrifice.

Gross anatomical inspection of post-mortem brains showed diffuse SAH in the ipsilateral hemisphere in 16/17 animals, and in 11 animals SAH also spread contralaterally [Fig. 2A(i)]. Examination of 5-mm coronal sections showed that clots had developed in the sulcus at the injection site in 12/17, and clots ranged 0.3 to 3.7 mm in maximal thickness (Fig. 2A). There was a greater likelihood of clots in animals with spreading depolarization clusters compared to animals with sparse or no spreading depolarization (7/7 versus 5/10; $P = 0.04$, Fisher's Exact Test), and clot thickness was also greater for animals with spreading depolarization clusters ($P < 0.01$, Mann-Whitney U-test) [Fig. 2A(iii)]. TTC staining further demonstrated cortical infarcts adjacent to sulcal clots in some animals [Fig. 2A(ii)]. Infarcts ranged from 3 to 10 mm in length along cortex and were more likely to occur in animals that had spreading depolarization clusters [5/7 (71%)] than those with sporadic or no spreading depolarization [2/10 (20%)]. This trend, however, did not reach significance with this sample size ($P < 0.06$, Fisher's Exact Test) [Fig. 2A(iv)]. Similarly, there was a strong trend toward thicker sulcal clots in animals with cortical infarcts [1.4 mm (0.9, 3.0)] than those without [0.3 mm (0.0, 1.3)] ($P < 0.06$, Mann-Whitney U-test).

Throughout the observation period, there were significant but not pathologically relevant changes in other monitoring variables, which remained in normal ranges. In 6 h, mean arterial pressure increased from 82 (75, 92) to 98 (87, 104) mmHg ($n = 17$, $P = 0.01$), intracranial pressure from 4.1 (3.6, 4.7) to 9.0 (7.3, 10.4) mmHg ($n = 11$, $P < 0.001$), cerebral perfusion pressure from 79 (69, 90) to 90 (73, 97) mmHg ($n = 11$, $P > 0.05$), and brain temperature from 36.6 (36.3, 37.2) to 38.8 (38.0, 38.8)°C ($n = 9$, $P < 0.01$, Mann-Whitney U-tests). Regional cerebral blood flow and $P_{bt}O2$ varied considerably but with insignificant net changes [rCBF: 31 (23, 37) to 24 (15, 40) ml/100 g/min ($n = 8$, $P > 0.05$); $P_{bt}O2$: 23 (7, 36) to 34 (11, 41) mmHg ($n = 11$, $P > 0.05$)]. An exception occurred in one animal, however, whose mean arterial pressure decreased progressively from 66 to 36 mmHg from the time of SAH until sacrifice, despite fluid resuscitation (Fig. 4). Repetitive spreading depolarizations in this animal became considerably prolonged and evolved into spreading, terminal depolarizations at some electrodes.

## Spreading depolarizations upregulate cyclooxygenase-2 expression in remote cortex

Spreading depolarizations do not typically cause cell death in otherwise normal cortex, but they do activate immediate

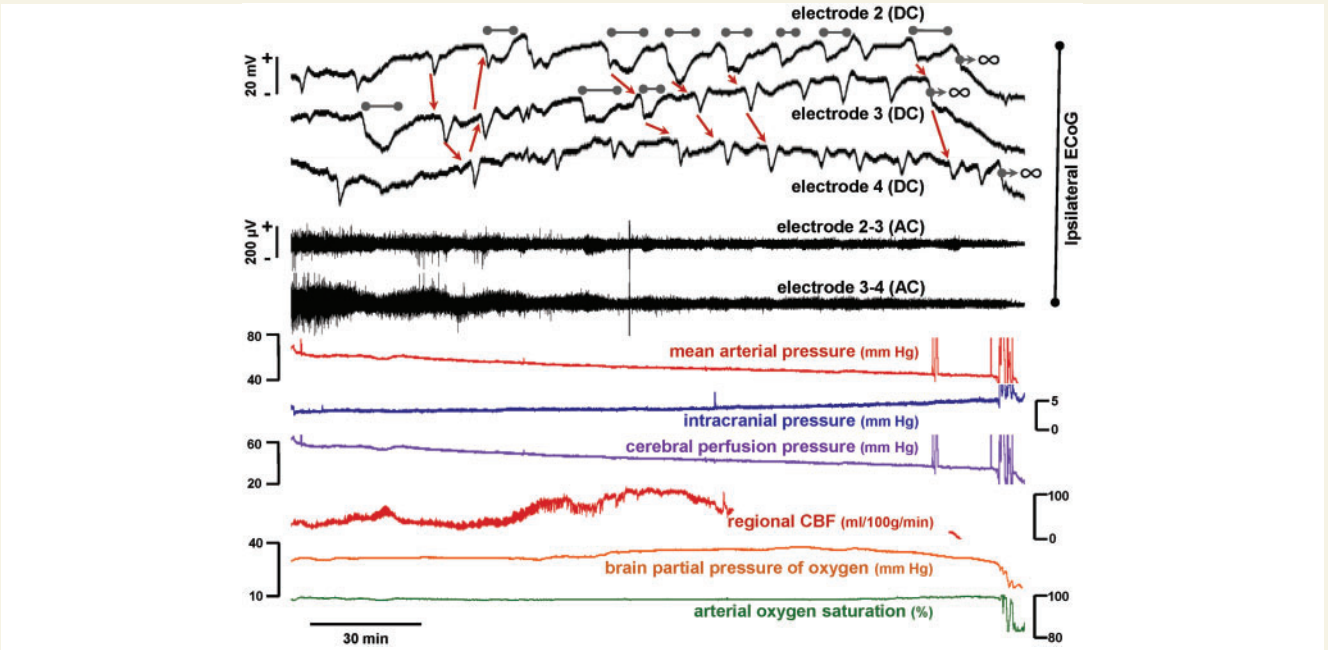


**Figure 4 Terminal spreading depolarizations following subarachnoid haemorrhage in the swine.** Top (black) traces show monopolar direct-current (DC) and bipolar high-frequency (alternating current, band-pass 0.5–50 Hz) ECoG recordings from the hemisphere ipsilateral to subarachnoid blood infusion. Beginning 7 min after SAH, ~12 spreading depolarizations were observed causing a progressive, cumulative depression of spontaneous brain activity to near isoelectricity. As denoted by grey bars, these spreading depolarizations became prolonged, with negative DC shifts lasting up to 10 min before recovery. The next spreading depolarization, observed spreading at a rate of 1.52 mm/min, was then terminal at Electrodes 2 and 3, as the DC shift did not recover [infinity symbols (∞) denote terminal depolarization], in contrast to recovery after 3 min at Electrode 4. After one further transient spreading depolarization at Electrode 4, however, the next event was terminal at this location. Thus, terminal depolarization developed in this cortical region in a spreading and progressive pattern through successive spreading depolarizations. The animal survived a further 2 h after this sequence until sacrifice. Arrows between DC shifts indicate presumed direction of spreading depolarization propagation between electrodes.

early genes and upregulate growth factors, stress response proteins, and inflammatory mediators (Sharp *et al.*, 2000; Jander *et al.*, 2001; Kunkler *et al.*, 2004; Urbach *et al.*, 2006). To investigate such effects of spreading depolarizations in cortex remote from developing lesions, we examined cyclooxygenase-2 (COX-2) expression in tissue 2 cm posterior to the SAH infusion site. COX-2 is an inducible, rate-limiting enzyme in prostaglandin synthesis that is upregulated by spreading depolarization (Koistinaho and Chan, 2000; Yokota *et al.*, 2003). In animals with spreading depolarization clusters, immunoblotting showed that COX-2 protein was significantly upregulated compared to homologous contralateral cortex where no spreading depolarizations occurred (Fig. 5A, $n = 5$, $P < 0.01$, paired *t*-test). The effect was not attributable to SAH alone or to experimental procedures, as there were no differences between hemispheres in animals with no spreading depolarization or even isolated spreading depolarizations ($n = 5$ and 3, respectively, $P$'s $> 0.30$, paired *t*-tests). Immunohistochemical staining confirmed COX-2 upregulation throughout upper cortical layers in the ipsilateral hemisphere of animals with spreading depolarization clusters (Fig. 5C). This pattern was observed not only in gyral crests but also along opposing cortices throughout the depths of sulci. No positive staining was observed in contralateral cortex of the same animals. COX-2 (*PTGS2*) upregulation occurred at the transcriptional level, as demonstrated by an ipsilateral increase in mRNA in animals with spreading depolarization clusters (Fig. 5B, $n = 5$, $P < 0.001$, paired *t*-test).

## Sulcal clots and cortical infarcts are modelled by subarachnoid infusion of clotted arterial blood

The above experiments demonstrated that subarachnoid infusion of fresh blood can be sufficient to induce spreading depolarization clusters and cortical infarction. However, this method failed to consistently model the clinical presentation of clot formation on the cortical surface or within sulcal depths; frequently the blood diffused widely to form only a thin layer. Therefore, in a second cohort ($n = 6$) we injected blood into the sulcus after clotting *ex vivo*. Free plasma haemoglobin in clotted blood at the time of injection was estimated as 0.46 (± 0.21) g/dl ($n = 5$), and one outlier was 2.81 g/dl. Sulcal infusion of 1 ml clotted blood caused spreading depolarizations in 5/6 animals with counts ranging from 4 to 20 in 6 h (Fig. 2D). In four

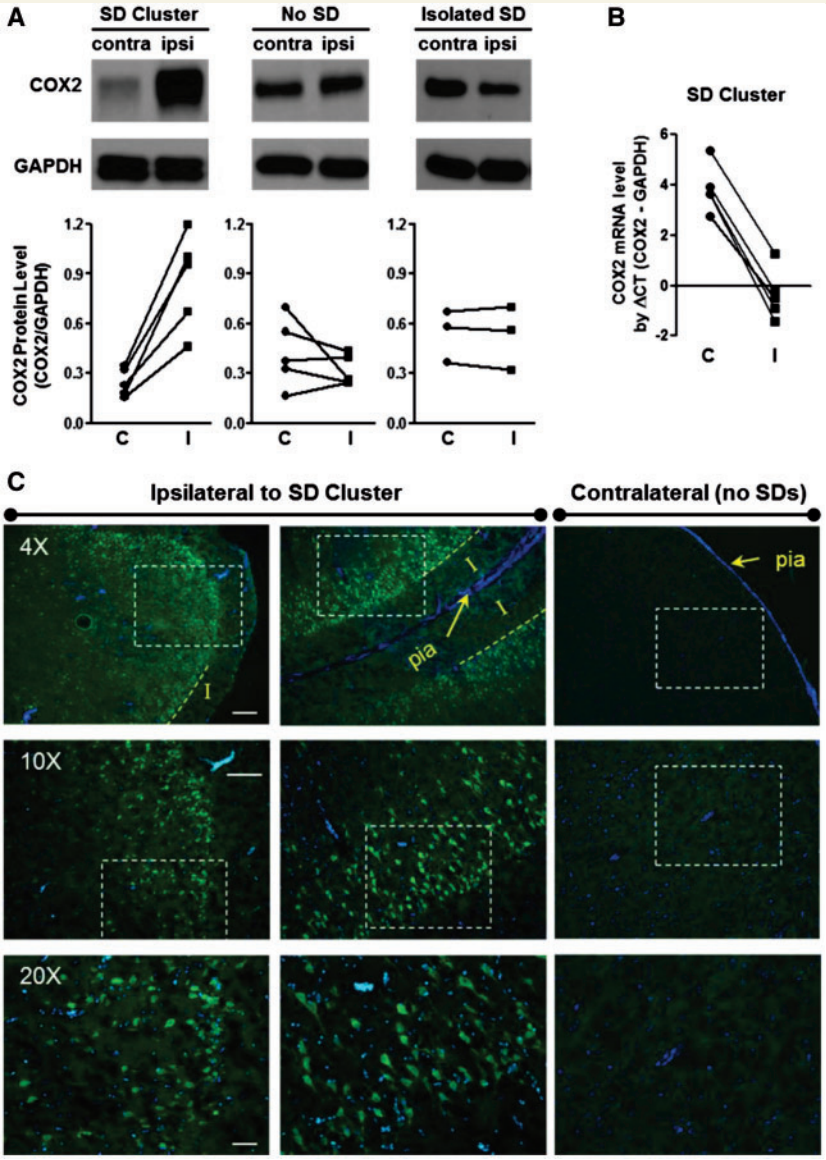


**Figure 5 Widespread hemispheric upregulation of COX-2 protein following spreading depolarization clusters.** (**A**) COX-2 protein expression in remote ipsilateral (I) and contralateral (C) cortex in animals with spreading depolarization (SD) clusters ($n = 5$), isolated spreading depolarizations ($n = 5$), and no spreading depolarizations ($n = 3$) in the hemisphere ipsilateral to subarachnoid haemorrhage. *PTGS2*/COX-2 levels were normalized to their endogenous control *GADPH* level. (**B**) COX-2 mRNA levels were measured by quantitative real-time PCR in the same tissue of animals with spreading depolarization clusters ($n = 5$). (**C**) Immunofluorescence staining of COX-2 protein level in viable ipsilateral and contralateral cortex 2 cm posterior to site of subarachnoid blood infusion. Strong positive neuronal staining was observed in superficial neuronal layers throughout gyral crests (*left*) and sulcal depths (*middle*) in the ipsilateral hemisphere, while no staining was observed on the contralateral side. Counterstaining of cell nuclei with DAPI. Scale bars = 250 (4×), 150 (10×), and 50 (20×) μm.

animals, electrode strips were placed along both medial and lateral gyri adjacent to the clotted sulcus. Of the total 43 spreading depolarizations in these animals, 40 were observed along both gyri, suggesting that spreading depolarizations cycle around the lesion in re-entrant patterns as shown previously in other models (Nakamura *et al.*, 2010; Santos *et al.*, 2014).

Injection of clotted blood resulted in consistent sulcal clot formation as demonstrated by post-mortem TTC staining (Fig. 2B). Maximal clot thickness was 5.9 mm (5.2, 6.6) and estimated volumes were 319 $mm^3$ (248, 351) ($n = 6$). Additionally, all animals in this cohort had substantial infarction through the full thickness of the cortex adjacent to the sulcal clot (Fig. 2B). Infarct volumes were 312 $mm^3$ (264, 736) ($n = 6$). In 3/6 animals, the infarct involved both the medial and lateral sides of the sulcus adjacent to the clot, as well as the connecting sulcal depth. The others had infarcts in a patchy pattern or on only one side of the sulcus. Some infarcts extended beyond the clots in the same sulcus, but never beyond the gyral crests. Histological examination of

these regions revealed well demarcated zones of vacuolization, consistent with oedema, and hypoxic-ischaemic neuronal cell injury (hypereosinophilic cytoplasm and nuclear pyknosis), consistent with acute infarction (Fig. 6). Congestion of small vessels, petechial haemorrhage, and infiltration of neutrophils were also noted.

To examine the roles of surgical dissection and mass effect in this model, a third cohort of animals was randomized to one of three experimental manipulations following surgical preparation: sulcal infusion of 1 ml normal saline ($n = 4$), fibrin sealant ($n = 4$), or 1 ml clotted blood ($n = 5$). TTC staining showed that thicknesses (blood versus fibrin: $3.3 \pm 1.2$ versus $4.4 \pm 2.0$ mm, *t*-test, $P = 0.38$) and volumes (blood versus fibrin: $128.8 \pm 44.3$ versus $179.8 \pm 148.0$ mm$^3$, *t*-test, $P = 0.55$) of sulcal masses did not differ between blood and fibrin clot groups. However, infarct volumes differed among the three groups [Fig. 2C, ANOVA, $F(2,10) = 7.35$, $P = 0.01$], with *post hoc* analysis (Bonferroni-Holm) showing a significant difference between blood and fibrin clot groups ($P < 0.05$), but not between fibrin and saline groups ($P = 0.36$). Spreading depolarizations occurred in all blood clot animals but in only one animal of both fibrin and saline groups (Fig. 2D). Statistical power (<27%, ANOVA) was inadequate to compare spreading depolarization counts between groups. However, across groups, spreading depolarization counts significantly correlated with cortical lesion volumes [Spearman's rank-order, $r_S(11) = 0.79$, $P < 0.01$].

## Early infarcts and spreading depolarizations in the acute phase after clinical aneurysmal subarachnoid haemorrhage

Based on experimental results, we investigated whether spreading depolarizations are more prevalent in aneurysmal

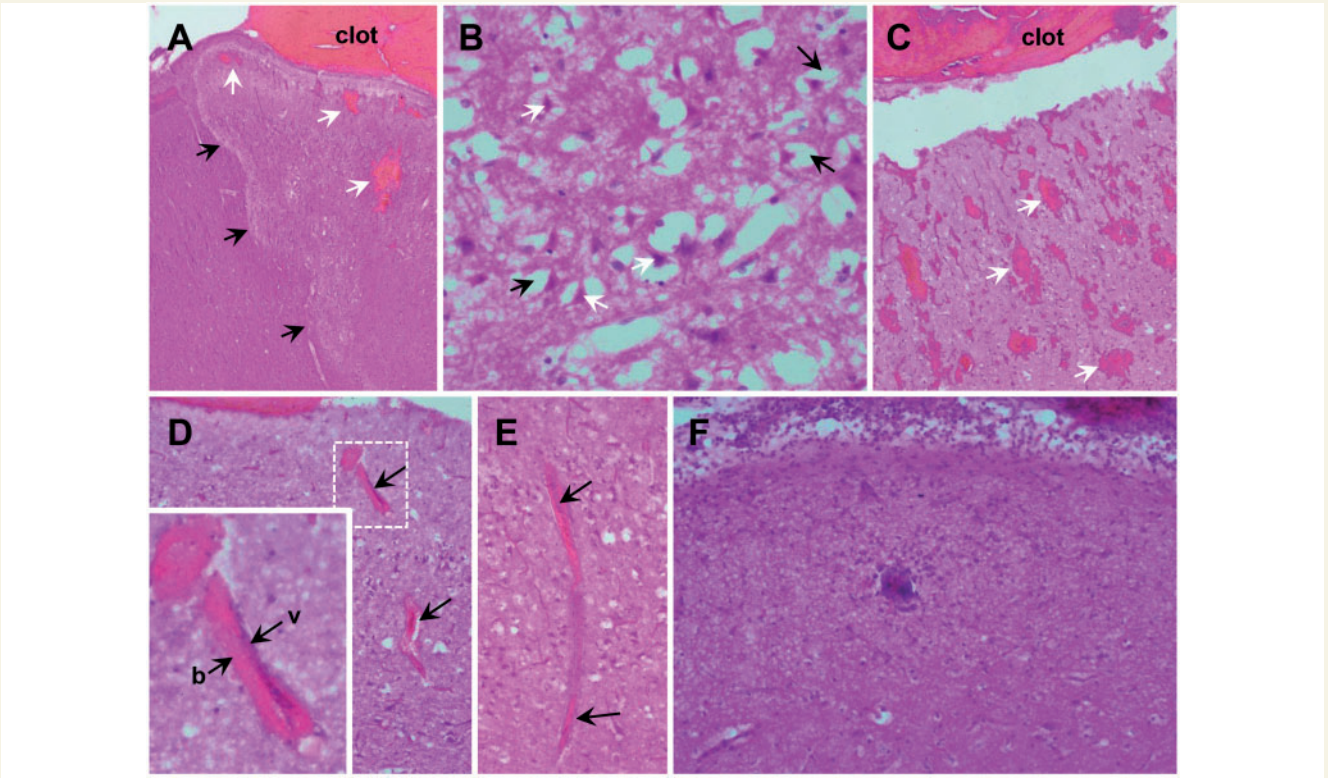


**Figure 6 Histologic sections of cortical ischaemia adjacent to sulcal subarachnoid clots.** (**A**) Zonal oedema (black arrows show borders) of cortex with intraparenchymal haemorrhage (white arrows) adjacent to subarachnoid clot (×40). Zones of ischaemic change were irregularly shaped, extending to involve the full cortical thickness. (**B**) Acute hypoxic-ischaemic neuronal cell injury (×400) is observed within these zones, as well as the immediately adjacent parenchyma, marked by pericellular vacuolization (black arrows) and neurons with scalloped morphology, pyknotic nuclei, and hyper-eosinophilic cytoplasm (white arrows). (**C**) Blood within perivascular spaces and extension into the adjacent parenchyma (petechial haemorrhages, white arrows) was seen focally in some cases and more prominently in others (×40). (**D**) In general, the extension of blood within perivascular (Virchow-Robin) spaces was more prominent within superficial cortex. Perivascular blood was present at least focally in all animals, but was prominent in some. The vessels (v) surrounded by blood (b) were frequently collapsed (×100, arrows and inset), as indicated by the lack of intravascular erythrocytes and lack of distinctive vessel walls. Congestion of the capillaries, microvasculature and small venules were present in the region of oedema. (**E**) A representative small venule with perivascular blood and collapse superficially (*top arrow*) with congestion noted in the deeper aspect (*bottom arrow*; ×100). (**F**) In nearly all animals, there was moderate to prominent layering of neutrophils (polymorphonuclear leucocytes) within the leptomeninges, with extension into the superficial parenchyma (×200). Occasional arteries also contained neutrophils with margination and, rarely, focal extravasation. No intravascular thrombi were identified.

SAH patients with early brain lesions compared to those without brain lesions. The clinical study was restricted to anterior communicating artery aneurysms to facilitate consistent assessment in a homogenous population, since these patients often develop characteristic ischaemic lesions along the interhemispheric fissure (Dreier *et al.*, 2002) and/or ICH in the frontal lobes. Twenty-three patients who underwent ECoG subdural electrode strip monitoring and early MRI assessment were included. Fourteen patients were female and the median age was 57 (47, 63) years. The aneurysm was treated by clip ligation in 14 patients and endovascular coil embolization in nine. Almost all patients showed Fisher grade 3 haemorrhage, and both the modified Hijdra Sum Score [19 (15, 27)] and the World Federation of Neurosurgical Societies (WFNS) grades [3 (1,5)] were relatively high for SAH studies. Patient characteristics are given in Table 1.

Continuous ECoG was recorded from subdural strips in the frontal lobe for a median duration of 54 (34, 66) h in individual patients during Days 0–3 after the initial haemorrhage. Eleven of 23 patients had a total of 222 spreading depolarizations during this period. The amplitude of the spreading depolarization identifying near-DC shift was 1.8 (1.5, 2.4) mV and the spreading depolarization propagation rate was 2.9 (2.5, 3.8) mm/min. Figure 7A shows an example of repetitive spreading depolarizations in Patient 4, which is an interesting case since spreading depolarizations became prolonged and evolved into persistent tissue depolarization.

MRIs were performed 24–48 h after aneurysm treatment on Day 2 (2, 3) after the initial haemorrhage. Four patients demonstrated a frontal ICH, another seven had an infarct in the proximal anterior cerebral artery territory (e.g. Fig. 7C), and one had both an infarct and ICH. The remaining 11 patients had no focal lesions. In patients with infarcts, there were no early signs of infarction or iatrogenic injury on initial CT scans performed 152 (86, 162) min after the estimated original haemorrhage ($n = 8$). By contrast, ICH lesions were visible on initial CT scans and were surrounded by a hypodense rim [111 (76, 121) min, $n = 4$]. Focal brain lesions were not attributable to aneurysm treatment method, since they occurred equally in patients undergoing clip ligation (50%, 7/14) and endovascular coil embolization (56%, 5/9) (Fisher Exact Test, $P = 1.0$). The global SAH burden (modified Hijdra Sum Score) was not significantly different between patients with and without a focal brain lesion [20 (16, 26), $n = 12$ versus (17 (14, 28), $n = 11$], but the local modified Hijdra Sum Score of the interhemispheric fissure, along which the infarcts were observed, was significantly higher in patients with a focal brain lesion [4.0 (3.8, 4.0) versus 3.0 (2.0, 3.5), Mann-Whitney U-test, $P = 0.045$].

Patients with focal brain lesions were significantly more likely to have spreading depolarizations (83%, 10/12) than those without focal brain lesions (9%, 1/11) (Fisher's Exact Test, $P < 0.001$). Accordingly, the peak spreading depolarizations/day of Days 0–3 was significantly higher in patients with focal brain lesions [12.6 (2.4, 20.3), $n = 12$, versus 0.0 (0.0,0.0), $n = 11$, Mann-Whitney U-test, $P < 0.001$]. Also, the ECoG depression periods (PTDDD) of Days 0–3 were significantly longer in patients with focal brain lesions than in those without [109.8 (20.4, 298.1), $n = 12$, versus 0.0 (0.0,0.0), $n = 11$, Mann-Whitney U-test, $P < 0.001$]. Mean baseline CPP [70 (68, 75), $n = 11$, versus 79 (74, 91), $n = 8$, $P = 0.035$] was significantly lower and baseline mean arterial pressure [83 (81, 86), $n = 12$, versus 94 (88, 100), $n = 11$, $P = 0.053$] trended toward lower values in patients with focal brain lesions. By contrast, no significant differences were found in ictal epileptiform event number or duration (*cf.* data in Table 1), or baselines of $P_{bt}O_2$ ($n = 8$ versus $n = 4$), intracranial pressure ($n = 11$ versus $n = 7$), brain temperature ($n = 7$ versus $n = 3$) or heart rate ($n = 12$ versus $n = 11$). Total recording times were also similar [56 (47, 84) versus 59 (39, 67) h].

When patients with (i) infarcts only ($n = 7$); (ii) with ICH only ($n = 4$); and (iii) without focal brain lesions ($n = 11$) were compared, both peak spreading depolarizations/day and PTDDD were significantly higher in patients with infarcts compared to patients without focal brain lesions (Kruskal-Wallis one-way ANOVA on ranks, Dunn's *post hoc* test, $P < 0.05$) (Fig. 7B). No significant differences were found between the other groups [peak spreading depolarizations/day: (i) 18.0 (1.9, 20.6); (ii) 11.4 (3.8, 21.1); (iii) 0.0 (0.0, 0.0); PTDDD: (i) 206.5 (20.6, 473.1); (ii) 83.8 (17.7, 182.5); (iii) 0.0 (0.0, 0.0)]. Clusters of spreading depolarizations, following the clinical definition of COSBID (Dreier *et al.*, 2017), were significantly more common in patients with infarcts only (4/7, 57%) than in patients without focal brain lesions (0/11, 0%) (Fisher's Exact Test, $P = 0.01$).

When patients with infarcts only ($n = 7$) and without focal brain lesions ($n = 11$) were compared, the WFNS was significantly higher [5.0 (4.0, 5.0) versus 1.0 (1.0, 2.0), Mann-Whitney U-test, $P = 0.004$] and the extended Glasgow Outcome Score after 6 months was significantly lower in patients with infarcts [1.0 (1.0, 2.5) versus 4.0 (3.0, 6.0), Mann-Whitney U-test, $P = 0.032$].

# Discussion

Our results confirm that the accumulation of subarachnoid blood is a sufficient pathological condition to acutely induce spreading depolarizations. Experimental infusion of fresh blood in the subarachnoid space triggered spreading depolarizations in 76% of animals and temporal clusters of repetitive spreading depolarizations in 41%. With fresh blood, the development of sulcal clots, and their thicknesses, were associated with greater spreading depolarization likelihood and recurrence. Cortical infarcts developed in 41% of animals, with a strong trend toward association with thicker clots and spreading depolarization clusters. Large, consistent clots were then produced in a subsequent cohort by sulcal injection of blood after *ex*

**Table 1 Characteristics of early brain injury in patients with anterior communicating artery aneurysmal SAH**

| No. | Age (years), sex | WFNS grade | Fisher grade | mHSS | mHSS (inter-hemispheric fissure) | Aneurysm treatment | Day of early MRI | Proximal ICH volume (ml) | Proximal ACA infarction volume (ml) | Distant infarction[a] | Peak SDs / day[b] | Peak isoelectric SDs / day[b] | PTDDD[b] | Peak total IEEs / day[b] | Peak total IEE duration / day[b] | Total recording time (min)[b] |
|---|---|---|---|---|---|---|---|---|---|---|---|---|---|---|---|---|
| 1 | 58, f | 2 | 3 | 29 | 4 | Coil | 3 | 0 | 0 | - | 0,0 | 0,0 | 0.0 | 0.0 | 0.0 | 1129 |
| 2 | 46, m | 2 | 3 | 14 | 4 | Coil | 2 | 34 | 0 | - | 0.0 | 0.0 | 0.0 | 0.0 | 0.0 | 3501 |
| 3 | 58, f | 1 | 3 | 30 | 3 | Coil | 1 | 0 | 0 | - | 0.0 | 0.0 | 0.0 | 0.0 | 0.0 | 4691 |
| 4 | 50, f | 3 | 3 | 27 | 4 | Clip | 2 | 0 | 7 | MCA | 34.7 | 9.6 | 647.3 | 0.0 | 0.0 | 3704 |
| 5 | 33, f | 1 | 3 | 15 | 3 | Coil | 4 | 0 | 0 | - | 0.0 | 0.0 | 0.0 | 0.0 | 0.0 | 116 |
| 6 | 62, m | 4 | 3 | 29 | 4 | Clip | 4 | 0 | 0 | - | 0.0 | 0.0 | 0.0 | 0.0 | 0.0 | 1118 |
| 7 | 46, f | 2 | 3 | 21 | 4 | Clip | 2 | 0 | 0 | - | 0.0 | 0.0 | 0.0 | 0.0 | 0.0 | 2242 |
| 8 | 77, f | 1 | 3 | 26 | 3 | Clip | 2 | 0 | 0 | - | 0.0 | 0.0 | 0.0 | 0.0 | 0.0 | 2506 |
| 9 | 58, f | 1 | 3 | 17 | 2 | Clip | 2 | 0 | 0 | - | 1.3 | 0.0 | 0.0 | 0.0 | 0.0 | 3585 |
| 10 | 49, m | 1 | 3 | 14 | 4 | Clip | 5 | 36 | 0 | Caudate nucleus | 5.0 | 0.0 | 23.6 | 6.7 | 15.3 | 2303 |
| 11 | 78, f | 4 | 3 | 16 | 2 | Clip | 1 | 41 | 0 | - | 17.8 | 0.0 | 144.1 | 189.4 | 239.2 | 1629 |
| 12 | 70, f | 4 | 3 | 20 | 3 | Coil | 2 | 0 | 35 | - | 1.0 | 0.0 | 11.1 | 0.0 | 0.0 | 4059 |
| 13 | 65, f | 5 | 3 | 32 | 4 | Clip | 3 | 0 | 10 | - | 21.0 | 7.0 | 886.9 | 0.0 | 0.0 | 4315 |
| 14 | 47, m | 5 | 3 | 27 | 4 | Clip | 3 | 0 | 156 | Hippo-campus | 2.9 | 0.0 | 30.1 | 0.0 | 0.0 | 2680 |
| 15 | 63, m | 5 | 3 | 19 | 4 | Coil | 1 | 77 | 4 | - | 7.5 | 0.0 | 75.4 | 0.0 | 0.0 | 4777 |
| 16 | 22, m | 2 | 3 | 12 | 2 | Coil | 2 | 0 | 0 | - | 0.0 | 0.0 | 0.0 | 0.0 | 0.0 | 4093 |
| 17 | 48, m | 5 | 3 | 16 | 1 | Coil | 0 | 0 | 8 | - | 20.1 | 0.0 | 206.5 | 0.0 | 0.0 | 4799 |
| 18 | 63, f | 5 | 3 | 16 | 4 | Clip | 2 | 0 | 13 | - | 0.0 | 0.0 | 0.0 | 0.0 | 0.0 | 1522 |
| 19 | 49, f | 4 | 4 | 20 | 4 | Clip | 2 | 0 | 56 | PCA | 18.0 | 0.0 | 298.8 | 0.0 | 0.0 | 2719 |
| 20 | 63, m | 1 | 1 | 14 | 1 | Clip | 3 | 0 | 0 | - | 0.0 | 0.0 | 0.0 | 0.0 | 0.0 | 1819 |
| 21 | 39, m | 4 | 3 | 26 | 4 | Coil | 1 | 16 | 0 | - | 31.2 | 22.3 | 297.8 | 0.0 | 0.0 | 3253 |
| 22 | 46, f | 1 | 3 | 8 | 1 | Clip | 1 | 0 | 0 | - | 0.0 | 0.0 | 0.0 | 2.9 | 5.5 | 3841 |
| 23 | 57, f | 5 | 3 | 13 | 2 | Clip | 2 | 0 | 0 | - | 0.0 | 0.0 | 0.0 | 0.0 | 0.0 | 3492 |

ACA = anterior cerebral artery; IEE = ictal epileptiform event; MCA = middle cerebral artery; mHSS = modified Hijdra Sum Score; PCA = posterior cerebral artery; SD = spreading depolarization; WFNS = World Federation of Neurological Surgeons.

[a]Anatomical structure or vascular territory outside the frontal lobe territory of the anterior cerebral artery.

[b]As scored from Days 0 to 3.

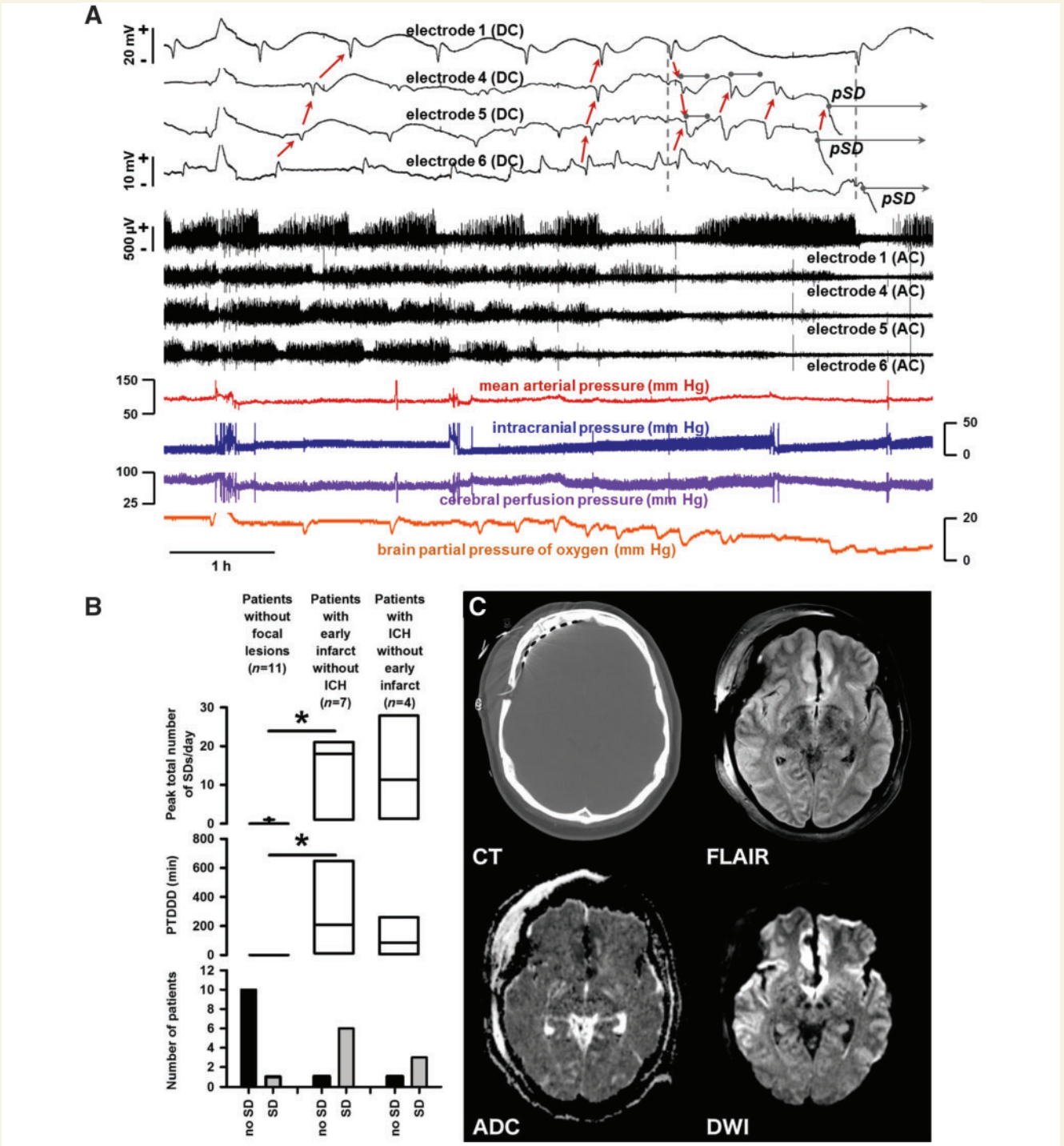


**Figure 7 Comparison of spreading depolarizations in patients with and without focal brain lesions.** (**A**) Evolution of spreading depolarizations in a patient with early cortical infarcts (Patient 4 in Table 1, *cf.* imaging in **C**) following rupture of an anterior communicating artery aneurysm. *Top traces* show raw direct current (DC, 0–45 Hz) recordings from four electrodes and *middle traces* show high frequency activity from the same electrodes (AC, 0.5–45 Hz). In the 7 h of multimodal monitoring shown, the patient displayed 13 spreading depolarizations across the electrode strip. The initial spreading depolarizations had short duration DC shifts and depression periods. Thereafter, recovery from depression periods is only partial at Electrodes 4–6 until spontaneous activity is completely and persistently depressed, i.e. isoelectric. Development of isoelectricity occurs progressively as a consequence of spreading depolarizations, as evidenced by propagating DC shifts (red arrows). Furthermore, prolongation of DC shifts is observed at Electrodes 4 and 5 (grey bars). Seventy-five minutes after the first prolonged DC shift, a persistent negative shift of DC potential (grey bar with arrow) develops in a spreading pattern from electrode 5→4. The propagation rate of this persistent spreading depolarization (pSD; 1.82 mm/min) is similar to the six spreading depolarizations that precede it (2.37 ± 0.88 mm/min). After a further 25 min, persistent depolarization then develops at Electrode 6; the event follows spreading depolarization on Electrode 1 with the same time delay as the prior spreading depolarization (vertical dashed lines), suggesting that it is also a spreading event. Throughout this course,

(continued)

*vivo* clotting, resulting in more complete infarction of surrounding cortex. Experimental results were translated in a focused clinical study of patients with ruptured anterior communicating artery aneurysms. Patients with early ischaemic lesions adjacent to interhemispheric SAH had an 86% incidence of spreading depolarizations from Days 0–3 post-haemorrhage compared to only 9% in patients without lesions. These results collectively suggest that spreading depolarizations are an early and persistent component of the pathophysiological response of cerebral cortex to the accumulation of subarachnoid blood and are likely involved in its subsequent progression to infarction.

Our results add evidence to a body of literature suggesting that spreading depolarizations are a ubiquitous and requisite mechanism of cortical infarction across a variety of diseases and animal models (Hartings *et al.*, 2017). The causal role of spreading depolarization is proven in focal ischaemic stroke, where initial terminal spreading depolarization triggers the persistent loss of ion homeostasis, intracellular $Ca^{2+}$ loading, glutamate efflux, and cytotoxic oedema in the ischaemic core, and spreading depolarizations arising spontaneously in the penumbra over subsequent hours induce the progressive expansion of terminally depolarized, and eventually infarcted, cortical tissue (von Bornstadt *et al.*, 2015). Similarly, when high $K^+$ and haemoglobin are topically applied to the cortex to mimic haemolysis as a model of delayed cerebral ischaemia after SAH, the occurrence of spreading depolarization, and consequent spreading ischaemia, are determining factors in infarct development (Dreier *et al.*, 2000, 2013; Hamming *et al.*, 2016). These concepts have now been translated to clinical conditions of traumatic brain injury, ischaemic stroke, ICH, and delayed cerebral ischaemia after SAH (Lauritzen *et al.*, 2011; Chung *et al.*, 2016). The present results extend these findings to the early period of ACI after SAH.

In early infarct development after SAH, we hypothesize that spreading depolarizations induce vasoconstriction (spreading ischaemia) and persistent cortical depolarization as requisite mechanisms leading to infarction. As direct evidence, we observed anecdotally in both swine and patients the delayed onset of persistent depolarization, which developed in a spreading pattern and was preceded by prolonged spreading depolarizations and the progressive, persistent deterioration of spontaneous cortical activity (Figs 4 and 7A). These patterns are hallmark, real-time diagnostic markers of lesion growth (Hinzman *et al.*, 2015; Dreier *et al.*, 2017; Hartings *et al.*, 2017). Furthermore, transient and cumulative decreases in $P_{bt}O_2$ in connection with spreading depolarizations, also seen anecdotally (Figs 3 and 7A), are strongly suggestive of vasoconstrictive responses to spreading depolarization (Dreier *et al.*, 2009; Bosche *et al.*, 2010). Nonetheless, a limitation of our swine study is that we did not specifically monitor the tissue fated for infarction to systematically investigate persistent depolarization and vasoconstriction. Electrodes rather were placed more remotely on the brain surface where cortex usually remained viable. On the other hand, this use of clinical methodology provided further evidence that detection of spreading depolarizations even in viable cortex signals the development of remote ischaemic zones (Dreier *et al.*, 2017), since spreading depolarizations were associated with infarction both experimentally and clinically. Spreading depolarizations are presumed to originate in or create these ischaemic zones, and their spreading nature allows their remote detection by ECoG strips that sample broad regions of cortex at high risk. Apart from this diagnostic advantage, it should not be neglected that spreading depolarizations have a strong effect on cellular function when they invade remote, viable cortex, as demonstrated here by COX-2 upregulation (Fig. 5). The widespread lobar or hemispheric effects of propagating spreading depolarizations are diverse and may include transient neurologic deficits, inflammation, neuroprotective preconditioning and neurogenesis (Gehrmann *et al.*, 1993; Kobayashi *et al.*, 1995; Dreier and Reiffurth, 2015; Urbach *et al.*, 2017).

An interesting question in the development of acute infarcts adjacent to subarachnoid clots is the causal relationship between spreading depolarizations and tissue ischaemia. One possibility is that SAH directly induces ischaemia through deprivation of blood flow, as in the endovascular puncture model (Busch *et al.*, 1998), and that spreading depolarization follows as a consequence. In our swine model, we similarly observed petechial cortical haemorrhage, which is likely caused by pressure from clots with sufficient volume and likely caused focal ischaemic hotspots. A purely compressive ischaemia is also possible, as suggested by the association of clot thickness with infarcts

**Figure 7** Continued

spreading depolarizations were coupled to transient decreases in $P_{bt}O_2$ as well as a stepwise cumulative decrease in baseline oxygenation from 21 to $<5$ mmHg. Large amplitude negative ultraslow potentials developed following persistent spreading depolarization at Electrodes 4–6 and returned to baseline levels after 2–3 h. (**B**, *bottom*) Only 1 of 11 patients without focal brain pathology showed a single spreading depolarization during Days 0–3 after the initial haemorrhage while the remaining 10 patients had no spreading depolarizations. By contrast, all but one patient with an early infarct and all but one patient with an initial ICH showed spreading depolarizations. Results were quantified by comparing the peak number of spreading depolarizations/day (*top*) and depression durations (PTDDD; *middle*). (**C**) Representative MRI on Day 2 of a patient with early infarct but not ICH. The CT displays the location of the electrode strip. DWI shows early band-like infarcts (hyperintensities) of the cortex and underlying white matter in the medial frontal area bilaterally (anterior cerebral artery territories), close to the ruptured anterior communicating artery aneurysm, as well as distant band-like infarcts in the left middle cerebral artery territory where the electrode strip was located. The fluid attenuated inversion recovery (FLAIR) image shows hyperintensities in these areas and the apparent diffusion coefficient (ADC) map shows hypointensities.

and spreading depolarizations. As evidence against this mechanism, experiments using thick fibrin clots to produce a sulcal mass effect did not cause infarcts significantly greater than saline controls. We note, however, that compressive ischaemia may require the presence of erythrocytes as a source for extravascular congestion and microvessel obstruction. This is suggested by observations in the blood clot model of erythrocyte infiltration into the perivascular space of arterioles and venules, in some cases causing complete vessel collapse (Fig. 6D and E). By comparison, models of acute subdural haematoma suggest that both compression from mass effect and blood constituents are required for cortical lesion development (Karabiyikoglu *et al.*, 2005; Baechli *et al.*, 2010). Finally, small cortical lesions were present in saline and fibrin clot control groups, demonstrating the presence of some ischaemic or iatrogenic injury even when spreading depolarizations did not occur.

Another possibility is that SAH directly triggers spreading depolarization by chemical mediators and that ischaemia develops primarily through spreading depolarization-induced spreading ischaemia. Spreading ischaemia is commonly observed in the human brain (Dreier *et al.*, 2009, 2017; Hinzman *et al.*, 2014) and can be sufficient for infarction (Dreier *et al.*, 2000, 2013). It is known that acutely haemolysed blood can directly trigger spreading depolarizations, an effect attributable to the high $K^+$ concentration of ~57 mM as shown, e.g. in mice (Oka *et al.*, 2017). In rats, the threshold concentration of subarachnoid $K^+$ inducing spreading depolarization is ~35 mM (causing a rise of intracortical extracellular $K^+$ from 3 to 6–9 mM) when blood is haemolysed at least partially, because extracellular haemoglobin scavenges nitric oxide (Dreier *et al.*, 1998) and decline in nitric oxide availability causes a marked reduction in the $K^+$ threshold for spreading depolarization *in vivo* and in brain slices (Petzold *et al.*, 2008). Here, free haemoglobin concentration of fresh and clotted blood at the time of injection was estimated at ~0.4–0.5 g/dl, corresponding to 250–310 μM, which is within the range sufficient for increasing the susceptibility to spreading depolarization and spreading ischaemia (Major *et al.*, 2017). Haemolysis may further accelerate in the *in vivo* environment after injection. For instance, the haemoglobin concentration peaked in subarachnoid haematomas both in humans and monkeys on the day of haemorrhage, with concentrations up to 30 g/dl (19 mM) in humans (Ohta *et al.*, 1980; Pluta *et al.*, 1998).

It should finally be considered that chemical and ischaemic induction of spreading depolarization are not exclusive alternatives, but in fact are complementary (Dreier *et al.*, 2002). Ischaemia reduces the threshold for chemical mediators to induce spreading depolarization, and vice versa, and these triggers may act in synergy without distinct boundaries. Furthermore, the relative roles of chemical and ischaemic mediators in inducing spreading depolarization, and of spreading depolarization-mediated vasoconstriction in creating tissue ischaemia, may vary through time and across the spatial gradient of developing lesions. In this regard, we note that in the swine model pannecrotic lesions can extend beyond the sulcal clot location and also occur in regions where petechial haemorrhage and vessel collapse were not observed, suggesting a key role of spreading depolarization and spreading ischaemia in expanding infarcts to the full extent observed. At the least, monitoring spreading depolarization provides a direct functional readout, useful for interventional studies and clinical translation, of the net effect of a variety of factors involved in damage evolution following SAH (Dreier *et al.*, 2017; Hartings, 2017).

Importantly, the swine studies establish a novel model of ACI after SAH. Typical experimental models of SAH use cisternal injection or vessel puncture but fail to replicate the time course of ACI and delayed cerebral ischaemia in patients, including ischaemic lesions (Marbacher *et al.*, 2010). Ischaemic neuronal injury was identified previously in a canine model of SAH, but did not constitute the extensive infarction observed here and was only observed after a week or longer (Jadhav *et al.*, 2008). Lesions in the non-human primate model can be similar to those in the swine model (Schatlo *et al.*, 2010), but ethical restrictions have precluded their further investigation. Furthermore, spontaneous spreading depolarizations do not appear to occur in rodent SAH models using cisternal blood injection, which presents a challenge for experimentalists (Chung *et al.*, 2016; Oka *et al.*, 2017). This is most likely because the small lissencephalic brains of rodents do not allow the focal accumulation of sufficient volumes of subarachnoid blood required for cortical infarction. Indeed, our results demonstrate that clot thickness is associated with greater risk and extent of infarction and suggest the importance of fissures and sulci for replicating the patho-anatomy of clinical SAH. The lesions observed in the swine sulcal clot model were similar to those described in patients as patchy or circumscript laminar infarcts adjacent to subarachnoid blood (Stoltenburg-Didinger and Schwarz, 1987; Dreier *et al.*, 2002; Weidauer *et al.*, 2008; Wagner *et al.*, 2013). In patients, thick layers of subarachnoid blood on admission CT scans are consistently among the most important predictors of infarction and unfavourable outcome after SAH (van Norden *et al.*, 2006; Rosen *et al.*, 2007).

# Conclusion

The present studies demonstrate that accumulation of blood in subarachnoid spaces of the gyrencephalic brain is sufficient to acutely cause patchy and band-like laminar infarction of adjacent cerebral cortex. The pathophysiology involves generation of repetitive spreading depolarizations, although the role of spreading depolarization and spreading ischaemia versus other mechanisms such as petechial haemorrhage and microvascular occlusion in causing ischaemic conditions remains to be determined. Clinical studies confirmed a strong association between spreading depolarizations and early brain lesions, including infarcts, adjacent to interhemispheric

SAH, and suggest the use of ECoG as a diagnostic for early brain injury that is often not observed on CT scans. Cortical infarcts in the period of ACI after aneurysmal SAH reflect secondary injury processes and may be preventable with therapies that target spreading depolarization and can be investigated in clinically relevant swine models.

## Acknowledgements

We thank Dr Ryszard Pluta for valuable advice and Austin Wanek for analysis of free haemoglobin.

## Funding

Studies were supported by the Mayfield Education and Research Foundation (J.A.H.); U.S. Department of Defense CDMRP PH/TBI Research Program (Project No. PT090526 to J.A.H.); Bundesministerium für Bildung und Forschung (Center for Stroke Research Berlin, 01 EO 080); the Deutsche Forschungsgemeinschaft (DFG DR 323/6-1 to J.P.D. and DFG DR 323/5-1 to J.P.D. and J.W.); National Institutes of Health (NIH)/National Institute of Neurological Disorders and Stroke (NINDS) (R00NS0 82379 to J.J.); NARSAD Young Investigator Grant from the Brain & Behavior Research Foundation (20940 to J.J.); Robert J. Dempsey, MD, Cerebrovascular Research Award of the Joint Section on Cerebrovascular Surgery of the AANS/CNS (to C.P.C.).

## Supplementary material

Supplementary material is available at *Brain* online.

## References

Ayata C, Lauritzen M. Spreading depression, spreading depolarizations, and the cerebral vasculature. Physiol Rev 2015; 95: 953–93.

Baechli H, Behzad M, Schreckenberger M, Buchholz HG, Heimann A, Kempski O, et al. Blood constituents trigger brain swelling, tissue death, and reduction of glucose metabolism early after acute subdural hematoma in rats. J Cereb Blood Flow Metab 2010; 30: 576–85.

Bosche B, Graf R, Ernestus RI, Dohmen C, Reithmeier T, Brinker G, et al. Recurrent spreading depolarizations after subarachnoid hemorrhage decreases oxygen availability in human cerebral cortex. Ann Neurol 2010; 67: 607–17.

Bretz JS, von Dincklage F, Woitzik J, Winkler MK, Major S, Dreier JP, et al. The Hijdra scale has a significant prognostic value for the functional outcome of Fisher grade 3 patients with subarachnoid hemorrhage. Clin Neuroradiol 2016. [Epub ahead of print]. doi: 10.1007/s00062-016-0509-0.

Broderick JP, Brott TG, Duldner JE, Tomsick T, Leach A. Initial and recurrent bleeding are the major causes of death following subarachnoid hemorrhage. Stroke 1994; 25: 1342–7.

Busch E, Beaulieu C, de Crespigny A, Moseley ME. Diffusion MR imaging during acute subarachnoid hemorrhage in rats. Stroke 1998; 29: 2155–61.

Chung DY, Oka F, Ayata C. Spreading depolarizations: a therapeutic target against delayed cerebral ischemia after subarachnoid hemorrhage. J Clin Neurophysiol 2016; 33: 196–202.

Claassen J, Carhuapoma JR, Kreiter KT, Du EY, Connolly ES, Mayer SA. Global cerebral edema after subarachnoid hemorrhage: frequency, predictors, and impact on outcome. Stroke 2002; 33: 1225–32.

de Haan B, Clas P, Juenger H, Wilke M, Karnath HO. Fast semi-automated lesion demarcation in stroke. Neuroimage Clin 2015; 9: 69–74.

De Marchis GM, Filippi CG, Guo X, Pugin D, Gaffney CD, Dangayach NS, et al. Brain injury visible on early MRI after subarachnoid hemorrhage might predict neurological impairment and functional outcome. Neurocrit Care 2015; 22: 74–81.

Dreier JP. The role of spreading depression, spreading depolarization and spreading ischemia in neurological disease. Nat Med 2011; 17: 439–47.

Dreier JP, Ebert N, Priller J, Megow D, Lindauer U, Klee R, et al. Products of hemolysis in the subarachnoid space inducing spreading ischemia in the cortex and focal necrosis in rats: a model for delayed ischemic neurological deficits after subarachnoid hemorrhage? J Neurosurg 2000; 93: 658–66.

Dreier JP, Fabricius M, Ayata C, Sakowitz OW, William Shuttleworth C, Dohmen C, et al. Recording, analysis, and interpretation of spreading depolarizations in neurointensive care: review and recommendations of the COSBID research group. J Cereb Blood Flow Metab 2017; 37: 1595–625.

Dreier JP, Korner K, Ebert N, Gorner A, Rubin I, Back T, et al. Nitric oxide scavenging by hemoglobin or nitric oxide synthase inhibition by N-nitro-L-arginine induces cortical spreading ischemia when $K^+$ is increased in the subarachnoid space. J Cereb Blood Flow Metab 1998; 18: 978–90.

Dreier JP, Major S, Manning A, Woitzik J, Drenckhahn C, Steinbrink J, et al. Cortical spreading ischaemia is a novel process involved in ischaemic damage in patients with aneurysmal subarachnoid haemorrhage. Brain 2009; 132 (Pt 7): 1866–81.

Dreier JP, Major S, Pannek HW, Woitzik J, Scheel M, Wiesenthal D, et al. Spreading convulsions, spreading depolarization and epileptogenesis in human cerebral cortex. Brain 2012; 135 (Pt 1): 259–75.

Dreier JP, Reiffurth C. The stroke-migraine depolarization continuum. Neuron 2015; 86: 902–22.

Dreier JP, Sakowitz OW, Harder A, Zimmer C, Dirnagl U, Valdueza JM, et al. Focal laminar cortical MR signal abnormalities after subarachnoid hemorrhage. Ann Neurol 2002; 52: 825–9.

Dreier JP, Victorov IV, Petzold GC, Major S, Windmuller O, Fernandez-Klett F, et al. Electrochemical failure of the brain cortex is more deleterious when it is accompanied by low perfusion. Stroke 2013; 44: 490–6.

Dreier JP, Windmuller O, Petzold G, Lindauer U, Einhaupl KM, Dirnagl U. Ischemia triggered by red blood cell products in the subarachnoid space is inhibited by nimodipine administration or moderate volume expansion/hemodilution in rats. Neurosurgery 2002; 51: 1457–65; discussion 65–7.

Dreier JP, Woitzik J, Fabricius M, Bhatia R, Major S, Drenckhahn C, et al. Delayed ischaemic neurological deficits after subarachnoid haemorrhage are associated with clusters of spreading depolarizations. Brain 2006; 129 (Pt 12): 3224–37.

Drenckhahn C, Brabetz C, Major S, Wiesenthal D, Woitzik J, Dreier JP. Criteria for the diagnosis of noninfectious and infectious complications after aneurysmal subarachnoid hemorrhage in DISCHARGE-1. Acta Neurochir Suppl 2013; 115: 153–9.

Drenckhahn C, Winkler MK, Major S, Scheel M, Kang EJ, Pinczolits A, et al. Correlates of spreading depolarization in human scalp electroencephalography. Brain 2012; 135 (Pt 3): 853–68.

Fisher CM, Kistler JP, Davis JM. Relation of cerebral vasospasm to subarachnoid hemorrhage visualized by computerized tomographic scanning. Neurosurgery 1980; 6: 1–9.

Gehrmann J, Mies G, Bonnekoh P, Banati R, Iijima T, Kreutzberg GW, et al. Microglial reaction in the rat cerebral cortex induced by cortical spreading depression. Brain Pathol 1993; 3: 11–17.

Hadeishi H, Suzuki A, Yasui N, Hatazawa J, Shimosegawa E. Diffusion-weighted magnetic resonance imaging in patients with subarachnoid hemorrhage. Neurosurgery 2002; 50: 741–7; discussion 7–8.

Hamming AM, Wermer MJ, Umesh Rudrapatna S, Lanier C, van Os HJ, van den Bergh WM, et al. Spreading depolarizations increase delayed brain injury in a rat model of subarachnoid hemorrhage. J Cereb Blood Flow Metab 2016; 36: 1224–31.

Hartings JA. Spreading depolarization monitoring in neurocritical care of acute brain injury. Curr Opin Crit Care 2017; 23: 94–102.

Hartings JA, Shuttleworth CW, Kirov SA, Ayata C, Hinzman JM, Foreman B, et al. The continuum of spreading depolarizations in acute cortical lesion development: examining Leao's legacy. J Cereb Blood Flow Metab 2017; 37: 1571–94.

Hertle DN, Dreier JP, Woitzik J, Hartings JA, Bullock R, Okonkwo DO, et al. Effect of analgesics and sedatives on the occurrence of spreading depolarizations accompanying acute brain injury. Brain 2012; 135 (Pt 8): 2390–8.

Hinzman JM, Andaluz N, Shutter LA, Okonkwo DO, Pahl C, Strong AJ, et al. Inverse neurovascular coupling to cortical spreading depolarizations in severe brain trauma. Brain 2014; 137 (Pt 11): 2960–72.

Hinzman JM, DiNapoli VA, Mahoney EJ, Gerhardt GA, Hartings JA. Spreading depolarizations mediate excitotoxicity in the development of acute cortical lesions. Exp Neurol 2015; 267: 243–53.

Hubschmann OR, Kornhauser D. Cortical cellular response in acute subarachnoid hemorrhage. J Neurosurg 1980; 52: 456–62.

Hubschmann OR, Kornhauser D. Effect of subarachnoid hemorrhage on the extracellular microenvironment. J Neurosurg 1982; 56: 216–21.

Jadhav V, Sugawara T, Zhang J, Jacobson P, Obenaus A. Magnetic resonance imaging detects and predicts early brain injury after subarachnoid hemorrhage in a canine experimental model. J Neurotrauma 2008; 25: 1099–106.

Jander S, Schroeter M, Peters O, Witte OW, Stoll G. Cortical spreading depression induces proinflammatory cytokine gene expression in the rat brain. J Cereb Blood Flow Metab 2001; 21: 218–25.

Karabiyikoglu M, Keep R, Hua Y, Xi G. Acute subdural hematoma: new model delineation and effects of coagulation inhibitors. Neurosurgery 2005; 57: 565–72; discussion 565–72.

Kobayashi S, Harris VA, Welsh FA. Spreading depression induces tolerance of cortical neurons to ischemia in rat brain. J Cereb Blood Flow Metab 1995; 15: 721–7.

Koistinaho J, Chan PH. Spreading depression-induced cyclooxygenase-2 expression in the cortex. Neurochem Res 2000; 25: 645–51.

Kunkler PE, Hulse RE, Kraig RP. Multiplexed cytokine protein expression profiles from spreading depression in hippocampal organotypic cultures. J Cereb Blood Flow Metab 2004; 24: 829–39.

Lagares A, Gomez PA, Lobato RD, Alen JF, Alday R, Campollo J. Prognostic factors on hospital admission after spontaneous subarachnoid haemorrhage. Acta Neurochir 2001; 143: 665–72.

Lauritzen M, Dreier JP, Fabricius M, Hartings JA, Graf R, Strong AJ. Clinical relevance of cortical spreading depression in neurological disorders: migraine, malignant stroke, subarachnoid and intracranial hemorrhage, and traumatic brain injury. J Cereb Blood Flow Metab 2011; 31: 17–35.

Lee JY, Keep RF, He Y, Sagher O, Hua Y, Xi G. Hemoglobin and iron handling in brain after subarachnoid hemorrhage and the effect of deferoxamine on early brain injury. J Cereb Blood Flow Metab 2010; 30: 1793–803.

Major S, Petzold GC, Reiffurth C, Windmuller O, Foddis M, Lindauer U, et al. A role of the sodium pump in spreading ischemia in rats. J Cereb Blood Flow Metab 2017; 37: 1687–705.

Marbacher S, Fandino J, Kitchen ND. Standard intracranial *in vivo* animal models of delayed cerebral vasospasm. Br J Neurosurg 2010; 24: 415–34.

Nakamura H, Strong AJ, Dohmen C, Sakowitz OW, Vollmar S, Sue M, et al. Spreading depolarizations cycle around and enlarge focal ischaemic brain lesions. Brain 2010; 133 (Pt 7): 1994–2006.

Neil-Dwyer G, Lang DA, Doshi B, Gerber CJ, Smith PW. Delayed cerebral ischaemia: the pathological substrate. Acta Neurochir 1994; 131: 137–45.

Ohta T, Kajikawa H, Yoshikawa Y, Shimizu K, Funatsu N, Yamamoto M. Cerebral vasospasm and hemoglobin: clinical and experimental studies. In: Wilkins RH, editor. Cerebral arterial spasm. Baltimore: Williams and Wilkins; 1980. p. 166–72.

Oka F, Hoffmann U, Lee JH, Shin HK, Chung DY, Yuzawa I, et al. Requisite ischemia for spreading depolarization occurrence after subarachnoid hemorrhage in rodents. J Cereb Blood Flow Metab 2017; 37: 1829–40.

Petzold GC, Haack S, von Bohlen Und Halbach O, Priller J, Lehmann TN, Heinemann U, et al. Nitric oxide modulates spreading depolarization threshold in the human and rodent cortex. Stroke 2008; 39: 1292–9.

Pluta RM, Afshar JK, Boock RJ, Oldfield EH. Temporal changes in perivascular concentrations of oxyhemoglobin, deoxyhemoglobin, and methemoglobin after subarachnoid hemorrhage. J Neurosurg 1998; 88: 557–61.

Rosen DS, Amidei C, Tolentino J, Reilly C, Macdonald RL. Subarachnoid clot volume correlates with age, neurological grade, and blood pressure. Neurosurgery 2007; 60: 259–66; discussion 66–7.

Sakowitz OW, Santos E, Nagel A, Krajewski KL, Hertle DN, Vajkoczy P, et al. Clusters of spreading depolarizations are associated with disturbed cerebral metabolism in patients with aneurysmal subarachnoid hemorrhage. Stroke 2013; 44: 220–3.

Santos E, Scholl M, Sanchez-Porras R, Dahlem MA, Silos H, Unterberg A, et al. Radial, spiral and reverberating waves of spreading depolarization occur in the gyrencephalic brain. Neuroimage 2014; 99: 244–55.

Sarrafzadeh AS, Sakowitz OW, Kiening KL, Benndorf G, Lanksch WR, Unterberg AW. Bedside microdialysis: a tool to monitor cerebral metabolism in subarachnoid hemorrhage patients? Crit Care Med 2002; 30: 1062–70.

Schatlo B, Dreier JP, Gläsker S, Fathi AR, Moncrief T, Oldfield EH, et al. Report of selective cortical infarcts in the primate clot model of vasospasm after subarachnoid hemorrhage. Neurosurgery 2010; 67: 721–9.

Schmidt JM, Rincon F, Fernandez A, Resor C, Kowalski RG, Claassen J, et al. Cerebral infarction associated with acute subarachnoid hemorrhage. Neurocrit Care 2007; 7: 10–17.

Schmidt V. Comparative anatomy of the pig brain—an integrative magnetic resonance imaging (MRI) study of the porcine brain with special emphasis on the external morphology of the cerebral cortex. Giessen, Germany: Justus Liebig University of Giessen; 2015.

Sehba FA, Bederson JB. Mechanisms of acute brain injury after subarachnoid hemorrhage. Neurol Res 2006; 28: 381–98.

Sharp FR, Lu A, Tang Y, Millhorn DE. Multiple molecular penumbras after focal cerebral ischemia. J Cereb Blood Flow Metab 2000; 20: 1011–32.

Stoltenburg-Didinger G, Schwarz K. Brain lesions secondary to subarachnoid hemorrhage due to ruptured aneurysms. In: Stroke and microcirculation. New York, NY: Raven Press; 1987. p. 471–80.

Terpolilli NA, Brem C, Buhler D, Plesnila N. Are we barking up the wrong vessels? Cerebral microcirculation after subarachnoid hemorrhage. Stroke 2015; 46: 3014–19.

Urbach A, Baum E, Braun F, Witte OW. Cortical spreading depolarization increases adult neurogenesis, and alters behavior and hippocampus-dependent memory in mice. J Cereb Blood Flow Metab 2017; 37: 1776–90.

Urbach A, Bruehl C, Witte OW. Microarray-based long-term detection of genes differentially expressed after cortical spreading depression. Eur J Neurosci 2006; 24: 841–56.

van Norden AG, van Dijk GW, van Huizen MD, Algra A, Rinkel GJ. Interobserver agreement and predictive value for outcome of two rating scales for the amount of extravasated blood after aneurysmal subarachnoid haemorrhage. J Neurol 2006; 253: 1217–20.

von Bornstadt D, Houben T, Seidel JL, Zheng Y, Dilekoz E, Qin T, et al. Supply-demand mismatch transients in susceptible peri-infarct hot zones explain the origins of spreading injury depolarizations. Neuron 2015; 85: 1117–31.

Wagner M, Steinbeis P, Guresir E, Hattingen E, du Mesnil de Rochemont R, Weidauer S, et al. Beyond delayed cerebral vasospasm: infarct patterns in patients with subarachnoid hemorrhage. Clin Neuroradiol 2013; 23: 87–95.

Wartenberg KE, Sheth SJ, Michael Schmidt J, Frontera JA, Rincon F, Ostapkovich N, et al. Acute ischemic injury on diffusion-weighted magnetic resonance imaging after poor grade subarachnoid hemorrhage. Neurocrit Care 2011; 14: 407–15.

Weidauer S, Vatter H, Beck J, Raabe A, Lanfermann H, Seifert V, et al. Focal laminar cortical infarcts following aneurysmal subarachnoid haemorrhage. Neuroradiology 2008; 50: 1–8.

Winkler MK, Dengler N, Hecht N, Hartings JA, Kang EJ, Major S, et al. Oxygen availability and spreading depolarizations provide complementary prognostic information in neuromonitoring of aneurysmal subarachnoid hemorrhage patients. J Cereb Blood Flow Metab 2017; 37: 1841–56.

Yokota C, Inoue H, Kuge Y, Abumiya T, Tagaya M, Hasegawa Y, et al. Cyclooxygenase-2 expression associated with spreading depression in a primate model. J Cereb Blood Flow Metab 2003; 23: 395–8.

Yun SP, Kim DH, Ryu JM, Park JH, Park SS, Jeon JH, et al. Magnetic resonance imaging evaluation of Yukatan minipig brains for neurotherapy applications. Lab Anim Res 2011; 27: 309–16.